

# Comparative analysis of the cyclic behaviour of beam-column joints with plain and deformed reinforcing bars

## Análise comparativa do comportamento cíclico de nós viga-pilar com armadura lisa e nervurada



C. FERNANDES<sup>a</sup>  
cfernandes@ua.pt

J. MELO<sup>b</sup>  
josemelo@ua.pt

H. VARUM<sup>c</sup>  
hvarum@ua.pt

A. COSTA<sup>d</sup>  
agc@ua.pt

### Abstract

Damage reports after recent earthquakes proves that slippage between steel reinforcing bars and the surrounding concrete is one the common causes of damage and collapse of existing RC building structures. The bond-slip mechanism assumes particular importance in RC building structures built until the 70's, with plain reinforcing bars, previously to the enforcement of modern seismic codes. This type of structures is usually characterized by poor reinforcement detailing, poor bond properties and inadequate concrete confinement. In RC buildings subjected to cyclic loads, as the induced by earthquakes, high stress concentration occurs at the beam-column joints, making this regions prone to the occurrence of severe damage. Beam-column joints are particularly sensitive to the bond-slip mechanism due to the stress concentration, but also due to the fact that anchorage of beam and column longitudinal reinforcing bars is typically made in the joint vicinity.

In this paper are presented the main results of the cyclic tests performed on two full-scale beam-column joints with the same geometry and reinforcement detailing, representative of interior joints in RC building structures built until the mid-70's, without adequate seismic detailing. One specimen was built with plain reinforcing bars (poor bond properties) and the other with deformed bars (good bond properties). For a better comprehension of the bond properties influence on the cyclic behavior of the beam-column joints, a comparison is established between the main experimental results obtained for the two specimens. The comparative analysis shows that the bond-slip mechanism has a strong influence in the cyclic response of RC structural elements.

**Keywords:** Beam-column joints; Cyclic behaviour; Concrete-steel bond; Plain reinforcing bars; Experimental tests.

### Resumo

Da observação dos danos provocados por diversos sismos recentes, verifica-se que o escorregamento aço-betão é uma das principais causas de dano e colapso de edifícios existentes de betão armado. Em muitos países, este fenómeno assume particular importância nos edifícios construídos até aos anos 70, com armadura lisa e anteriormente à introdução dos primeiros regulamentos que contemplam a acção sísmica com maior detalhe. Este tipo de estruturas apresenta, geralmente, pormenorização deficiente da armadura, fracas condições de aderência e confinamento inadequado do betão. As ligações viga-pilar nas estruturas de betão armado são pontos onde ocorrem danos significativos quando as estruturas estão sujeitas a carregamentos cíclicos, uma vez que nestas zonas ocorre a maior concentração de esforços. O fenómeno do escorregamento assume particular relevância nas ligações viga-pilar, devido aos maiores esforços que aqui se desenvolvem mas também ao facto de nestas zonas se realizar tipicamente a ancoragem dos varões longitudinais dos pilares e/ou vigas.

Neste artigo são apresentados os principais resultados dos ensaios cíclicos de dois nós viga-pilar à escala real com igual geometria e igual pormenorização da armadura, representativos de nós interiores de edifícios de betão armado construídos até meados dos anos 70 sem pormenorização adequada para fazer face à acção sísmica. Um dos nós foi construído com armadura lisa (com fracas condições de aderência) e o outro nó com armadura nervurada (com boas condições de aderência). Faz-se também a comparação dos resultados obtidos para compreender a influência das condições de aderência na resposta cíclica de nós interiores viga-pilar deste tipo de estruturas de betão armado. Dos resultados obtidos, conclui-se que o fenómeno do escorregamento condiciona significativamente o desempenho das estruturas com armadura lisa quando solicitadas por acções cíclicas.

**Palavras-chave:** Nós viga-pilar; Comportamento cíclico; Aderência aço-betão; Armadura lisa; Ensaios experimentais.

<sup>a</sup> University of Aveiro, Civil Engineering Department, cfernandes@ua.pt, Campus Universitário de Santiago, 3810-193 Aveiro, Portugal;

<sup>b</sup> University of Aveiro, Civil Engineering Department, josemelo@ua.pt, Campus Universitário de Santiago, 3810-193 Aveiro, Portugal;

<sup>c</sup> University of Aveiro, Civil Engineering Department, hvarum@ua.pt, Campus Universitário de Santiago, 3810-193 Aveiro, Portugal;

<sup>d</sup> University of Aveiro, Civil Engineering Department, agc@ua.pt, Campus Universitário de Santiago, 3810-193 Aveiro, Portugal.

### 1. Introduction

An important number of existing reinforced concrete (RC) building structures, located in seismic-prone countries, were built until the mid-1970s, with plain reinforcing bars, before the introduction of adequate seismic-oriented design codes. Observation on the performance of existing RC structures during recent earthquakes (Sichuan, China 2008; L'Aquila, Italy 2009; Port-au-Prince, Haiti 2010; Concepción, Chile 2010) confirm their high vulnerability to seismic loads.

The hysteretic behavior of RC structures is highly dependent on the interaction between steel and concrete. Perfect bond is usually assumed in the analyses of reinforced concrete structures, implying full compatibility between concrete and reinforcement strains. However, this assumption is only valid for early loading stages and low strain levels. As the loads increases, cracking and breaking of bond unavoidably occurs and relative slip between the concrete and the reinforcing bars (bond-slip) takes place in the structural elements. Consequently, different strains are observed in the steel bars and in the surrounding concrete, and the stress distribution is affected in both materials [1]. Under cyclic load reversals, like the ones induced by earthquakes, concrete-steel bond experienc-

es progressive degradation that leads to significant bar slippage. Bond-slip effects are particularly significant in elements built with plain reinforcing bars, to which are associated poor bond properties. This process can lead to failure at a cyclic stress level lower than the ultimate stress under monotonic loading [2]. Loss of bond between reinforcing bars and the surrounding concrete has been reported as a common cause of severe local damage and even collapse of many structures during strong earthquakes. Associated to other detailing deficiencies (e.g. deficient amount or absence of joint shear reinforcement, poor anchorage detailing of the beam and column reinforcement, among others), poor bond conditions in beam-column joints often lead to a brittle failure of the connections and, consequently, of the whole structure.

The majority of experimental studies on the cyclic behavior of RC elements (like the ones described in [3]), refer to elements with deformed bars. Consequently, the influence of plain reinforcing bars on the non-linear response of elements and critical regions (like beam-column joints) is not fully established [4]. Reports of recent experiments made on elements with plain reinforcing bars can be found, for example, in [5,6,7] (pull-out tests for investigating the concrete-steel bond behavior), [8,9,10,11] (structural elements) and [1,12,13] (frames).

Figure 1 – Test specimens (JP and JD): a) structural scheme and support conditions idealized; b) geometry; c) cross-sections and reinforcement detailing; d) longitudinal reinforcing details

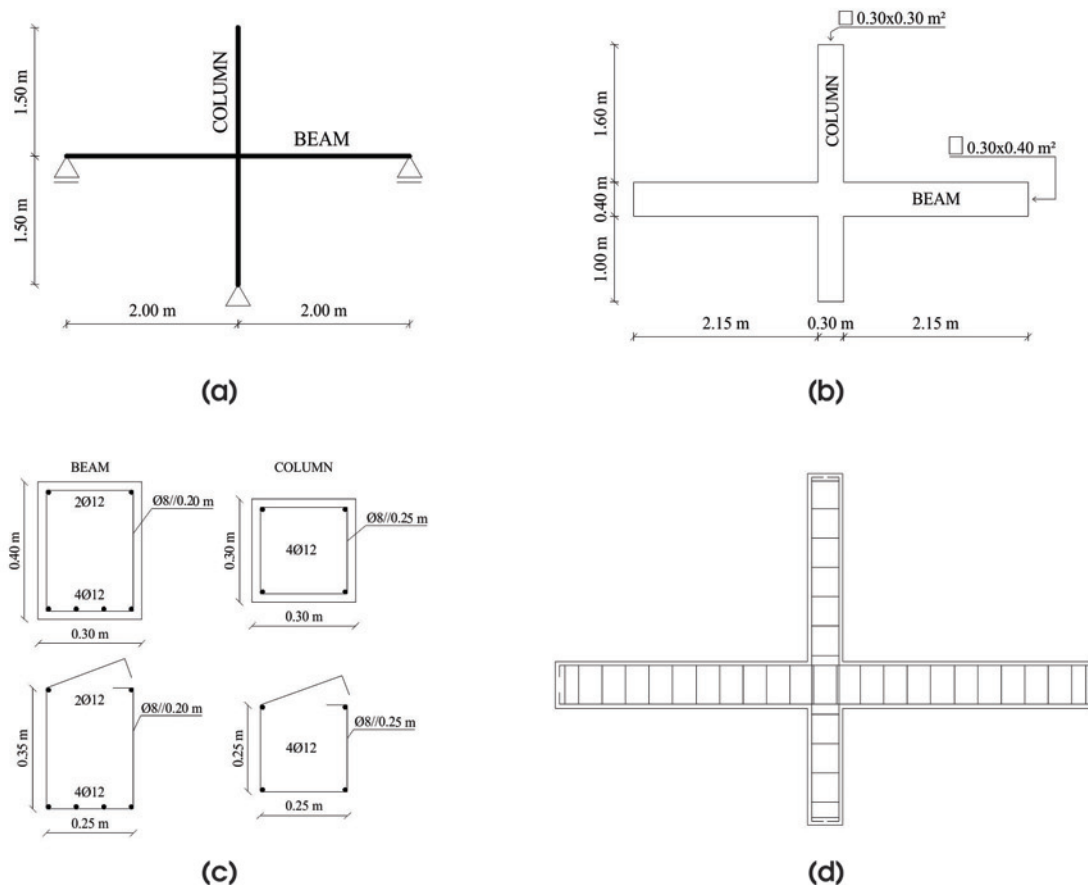


**Table 1 – Steel mechanical properties (mean values)**

Material	Property	Value
Plain bars	Yielding strength $f_{y,l}$ (MPa)	590
	Ultimate strength $f_{u,n}$ (MPa)	640
	Elastic modulus $E_{y,l}$ (GPa)	198
Deformed bars	Yielding strength $f_{y,l}$ (MPa)	430
	Ultimate strength $f_{u,n}$ (MPa)	550
	Elastic modulus $E_{y,n}$ (GPa)	200

In terms of analytical and numerical models for describing the concrete-steel bond behavior (which is usually made in terms of a bond stress-slip relationship), the majority was developed for specimens with deformed bars (see [3,14]). The model described in [15], based on the bond stress-slip relationship developed by Eligehausen *et al.* [16], is the most widely used for elements with plain reinforcing bars. A hysteretic bond stress-slip relationship for describing bond behavior on elements with plain reinforcing bars was recently proposed by Verderame *et al.* [17].

According to several authors (like [1,9,10,11,18]), considering the bond-slip mechanism in the numerical models of structural analysis is a necessary enhancement towards a realistic description of the cyclic behavior and the ultimate capacity of reinforced concrete structures, namely when plain reinforcing bars are used.

In this paper are presented the main experimental results of the cyclic tests performed on two full-scale beam-column joints [19],

**Figure 2 – Test setup: a) support and loading conditions idealized; b) schematics; c) general view**

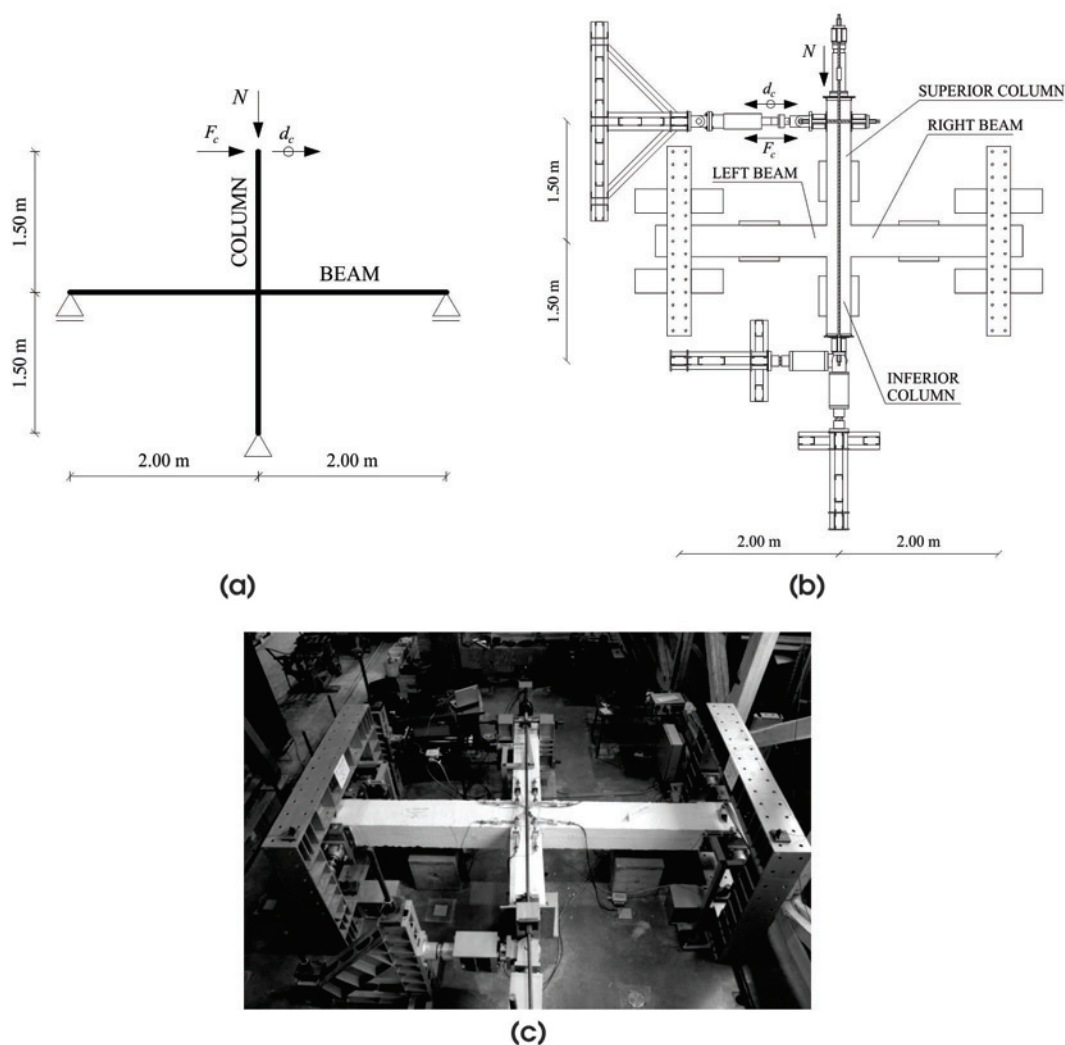
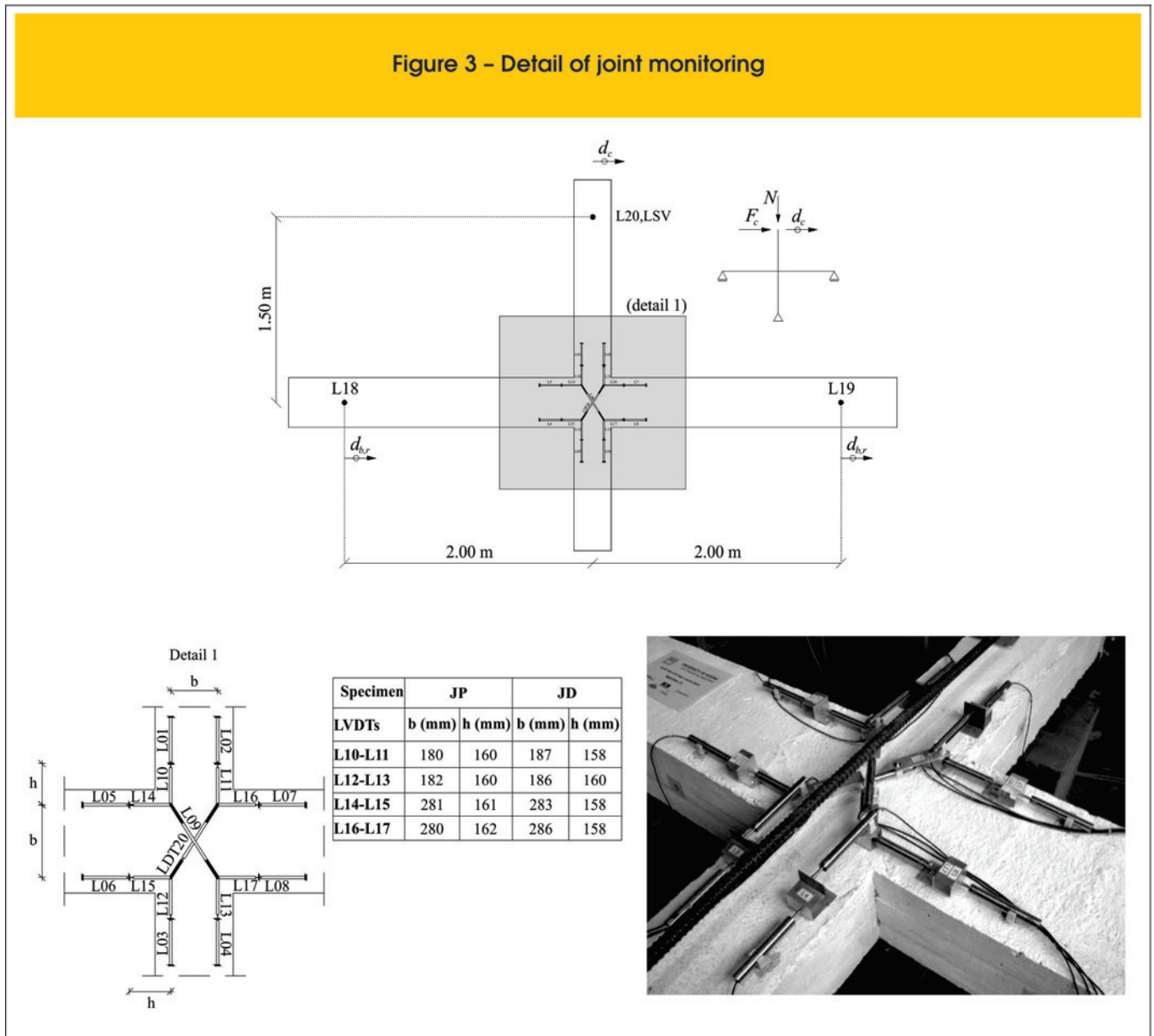


Figure 3 – Detail of joint monitoring



representative of typical interior beam-column joints in existing RC building structures built until the mid-1970s without adequate reinforcement detailing for seismic loading. The two specimens have the same geometry and reinforcement detailing. One specimen was built with plain reinforcement bars and the other specimen was built with deformed bars. Whenever possible, the experimental results of the two specimens are plotted together for better understanding how the bond-slip mechanism influences the joints performance.

## 2. Cyclic tests of beam-column joints

### 2.1 Test specimens

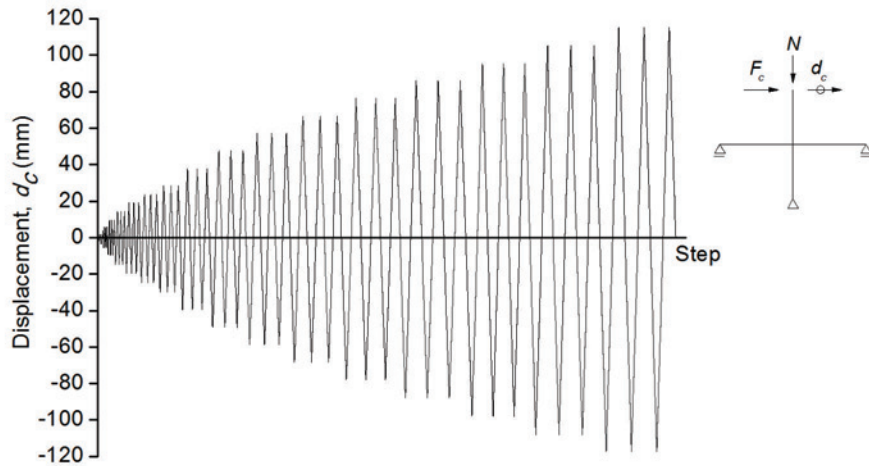
In Figure 1 are represented the specimens' geometry, support conditions idealized and the reinforcement detailing. The two

specimens have the same geometry, dimensions and reinforcement detailing, and were cast at the same time. They simulate the connection between two beams with 0.30x0.40 m<sup>2</sup> cross section and span equal to 4 m, and two columns with 0.30x0.30 m<sup>2</sup> cross-section and storey height of 3 m. Specimen JP was built with plain reinforcing bars and specimen JD was built with deformed bars.

The beam longitudinal reinforcement is constituted by two bars at the top and four bars at the bottom, all with 12 mm diameter. The transverse reinforcement is constituted by 8 mm stirrups distanced by 0.20 m. The column longitudinal reinforcement is constituted by four bars with 12 mm diameter (one at each corner) and the transverse reinforcement is constituted by 8 mm stirrups distanced by 0.25 m. The concrete cover in the beams and column is equal to 2 cm.

The steel mechanical properties are presented in Table 1. The mechanical properties of the plain reinforcement bars were determined resorting to tensile strength tests. Since bar samples of

Figure 4 - Displacement history



deformed steel were not available for tensile strength testing, the mean values of the mechanical properties of S400 steel class (the steel class used in the construction of the specimens) were adopted. Compressive tests of concrete cubic samples ( $15 \times 15 \times 15 \text{ cm}^3$ ), cast together with the specimens, were made for determining the concrete compressive strength. A mean strength ( $f_{cm}$ ) equal to 23.5 MPa was obtained. The characteristic compressive strength was estimated according to the standard EN 206-1 [20] and is equal to 19.5 MPa, corresponding to the C16/C20 concrete class according to the Eurocode 2 [21] classification.

## 2.2 Test procedure

In Figure 2 are illustrated the test setup adopted and the idealized support and loading conditions. Two hydraulic actuators were arranged at the top of the column, one to impose the lateral displacements ( $d_c$ ) and the other for the axial force ( $N$ ). The specimens were tested in the horizontal position. Four high load-carrying capacity devices with reduced friction were placed below the specimens to carry their self-weight. Steel reaction frames associated to sliding devices at the beam extremities were used to simulate the beams support conditions, allowing displacements only in the longitudinal direction of the beam and in-plane rotations. The frictional forces due to the devices used to support the specimens' weight and to simulate the beams supports are insignificant, corresponding only to about 2.5% of the maximum load imposed.

LVDTs (Figure 3) were used for measuring the global displacements at the top of the column ( $d_c$ ) and at the beam left and right supports ( $d_{b,l}$  and  $d_{b,r}$  respectively), as well as the local relative displacements in the beam-joint and column-joint interfaces, and joint, for monitoring the local deformation and crack evolution. Two load cells were placed at the column's pinned support for monitoring the reaction forces there developed.

The test was made under displacement-controlled conditions. The two specimens were subjected to the same lateral displacement history, imposed to the top of the columns. The displacement history, depicted in Figure 4, consists of a series of three push-and-pull cycles per each level of displacement. Eighteen (18) displacement levels of increasing amplitude were adopted until a maximum of 120 mm (4% drift). The two specimens were subjected to the same level of column axial force, equal to 200 kN, corresponding to a normalized axial force approximately equal to 10%. During the cyclic tests, the axial force variation was monitored. It was observed a small reduction in the axial force was registered for both specimens, with a maximum variation of 5% and 3% for specimen JP and JD, respectively, relatively to the initial value imposed. Even if is small, this reduction is justified by the stiffness degradation associated to the damage evolution.

Figure 5 - Force-displacement diagrams

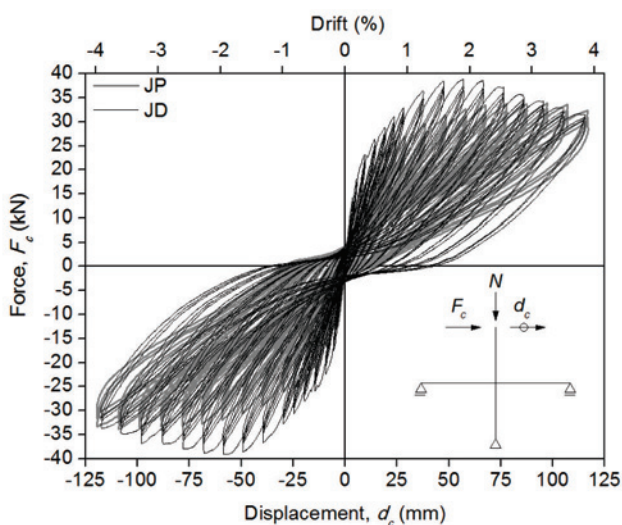
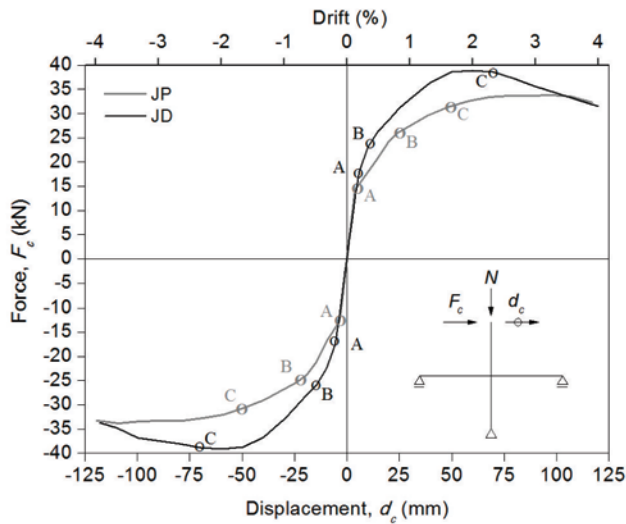


Figure 6 - Peak envelopes and damage identification



**Legend:**  
 A - Beginning of concrete cracking in the beams  
 B - Beginning of concrete cracking in the columns  
 C - Beginning of concrete cover spalling in the beams (specimen JP) and in the columns (specimen JD)

### 3. Experimental results

In this section are presented the main experimental results for specimens JP and JD, namely the force-displacement and the moment-curvature diagrams, evolution of the total dissipated energy and damage evolution. The experimental results of the two specimens are plotted together for better understanding the differences between their behavior.

Figure 7 - Evolution of the total dissipated energy

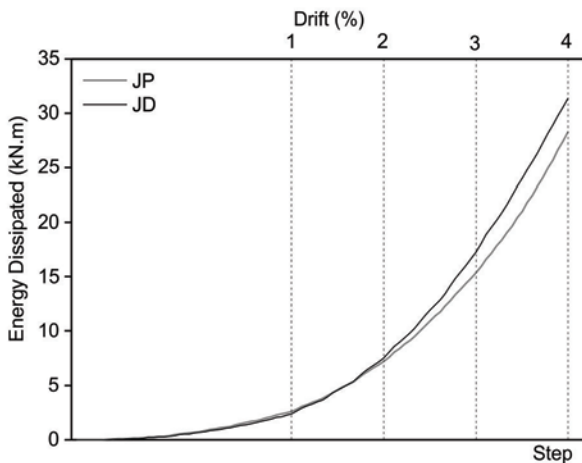


Table 2 - Dissipated energy for each drift level

$\Delta_{i,i+1}$	Specimen JP		Specimen JD	
	$E_{i,i+1}$ (kN·m)	$E_{i,i+1}$ (%)	$E_{i,i+1}$ (kN·m)	$E_{i,i+1}$ (%)
$\Delta_{0,1}$	2.61	9	3.39	11
$\Delta_{1,2}$	4.61	16	4.13	13
$\Delta_{2,3}$	8.19	29	9.78	31
$\Delta_{3,4}$	12.90	46	14.06	45

#### 3.1 Force-displacement, dissipated energy and moment-curvature diagrams

In Figure 5 is shown the force-displacement/drift diagrams for the two specimens under analysis. The corresponding peak envelopes, with identification of the beginning of cracking and concrete spalling in the beam and column, are presented in Figure 6. The evolution of the total energy dissipated by each specimen during the experimental test is represented in Figure 7. In Table 2 are presented the values of dissipated energy ( $E_{i,i+1}$ ) for different drift levels ( $D_{i,i+1}$ ) and the percentage that each value represents in relation to the total dissipated energy. Figure 8 shows the moment-curvature relationship computed for the beam-joint and column-joint interfaces. For each case, the curvatures represented correspond to mean values of curvature estimated for the first slice in the corresponding element. The mean curvature in a given slice is obtained by dividing the relative rotation between the two extremity sections by the length of the slice (distance between the fixation points of the LVDTs, considered equal to  $h$ , Figure 3). The relative rotation between the two extremity sections is computed as the quotient between the difference between the readings from the two LVDTs and the distance between them ( $b$ , Figure 3).

In terms of global behavior, the specimen built with plain reinforcing bars reaches the maximum strength for a lateral force equal to 34 kN, in both directions, as shown in Figures 5 and 6. In the positive direction the maximum force was registered at  $D = \pm 100\text{mm}$  (3.3% drift). In the negative direction the maximum force was registered  $D = \pm 110\text{mm}$  (3.7% drift). The specimen with deformed reinforcing bars reached the maximum strength for a lateral force equal to 39 kN at  $D = \pm 60\text{mm}$  (2.0% drift), in both directions. At the end of the test ( $D = \pm 120\text{mm}$ , 4% drift), the lateral force in specimen JP is about 95% (positive direction) and 98% (negative direction) of the maximum value achieved during the test. This result indicates that elements built with plain reinforcing bars have small strength degradation, even for larger levels of deformation. For specimen JD, the maximum lateral force registered at the end of the test is about 81% (positive direction) and 86% (negative direction) of the maximum force achieved during the test.

In terms of damage evolution, in the two specimens the cracking was initiated at the beam-joint interfaces for a displacement equal to  $D = \pm 4\text{mm}$ . At  $D = \pm 24\text{mm}$  for specimen JP, and  $D = + 10\text{mm}$  and  $D = -14\text{mm}$  for specimen JD, cracks were developed at the

column-joint interfaces. For specimen JP, spalling of the concrete cover occurred for lower drift levels than for specimen JD.

Establishing the comparison between the results for the two specimens, the following conclusions can be drawn: i) the maximum strength achieved by specimen JP corresponds to 87% of the maximum strength of specimen JD; ii) specimen JD achieves its maximum strength for a lower drift level than specimen JP; iii) as expected, the initial uncracked stiffness is similar in both specimens; iv) after cracking onsets, and for larger drift levels, specimen JP displays lower stiffness than specimen JD.

Regarding the energy dissipation capacities, the total dissipated energy for specimens JP and JD was equal to 28.31 kN×m and 31.37 kN×m, respectively. In other words, the total energy dissipated by specimen JP is 10% lower than the total energy dissipated by specimen JD. Until 2% drift the evolution of dissipated energy is similar for both specimens, being slightly superior for specimen JP. For drift levels superior to 2%, the total energy dissipation in specimen JD increases significantly.

The moment-curvature diagrams represented in Figure 8-a and 8-b show that this relationship is similar for the column sections of the two specimens. The maximum moment is equal to 43 kN×m and 50 kN×m for specimens JP and JD, respectively. Regarding the beam sections Figures 8-c and 8-d, the peak envelopes of the moment-curvature diagrams are not symmetric since the superior and inferior longitudinal reinforcement are asymmetrical. The maximum moment is equal to 63 kN×m and -32 kN×m for specimen JP, and 71 kN×m and -37 kN×m for specimen JD. The lowest curvature values were estimated for the left beam section of specimen JD due to the small values of crack opening registered at this region (see Figure 13-c).

### 3.2 Damage evolution

In Figures 9 and 10 is shown the final damage state observed in specimens JP and JD, respectively. In specimen JP, cracks and concrete cover spalling are concentrated at the beam-joint and

**Figure 8 - Moment-curvature diagrams computed at the: a) superior column-joint interface; b) inferior column-joint interface; c) left beam-joint interface; d) right beam-joint interface**

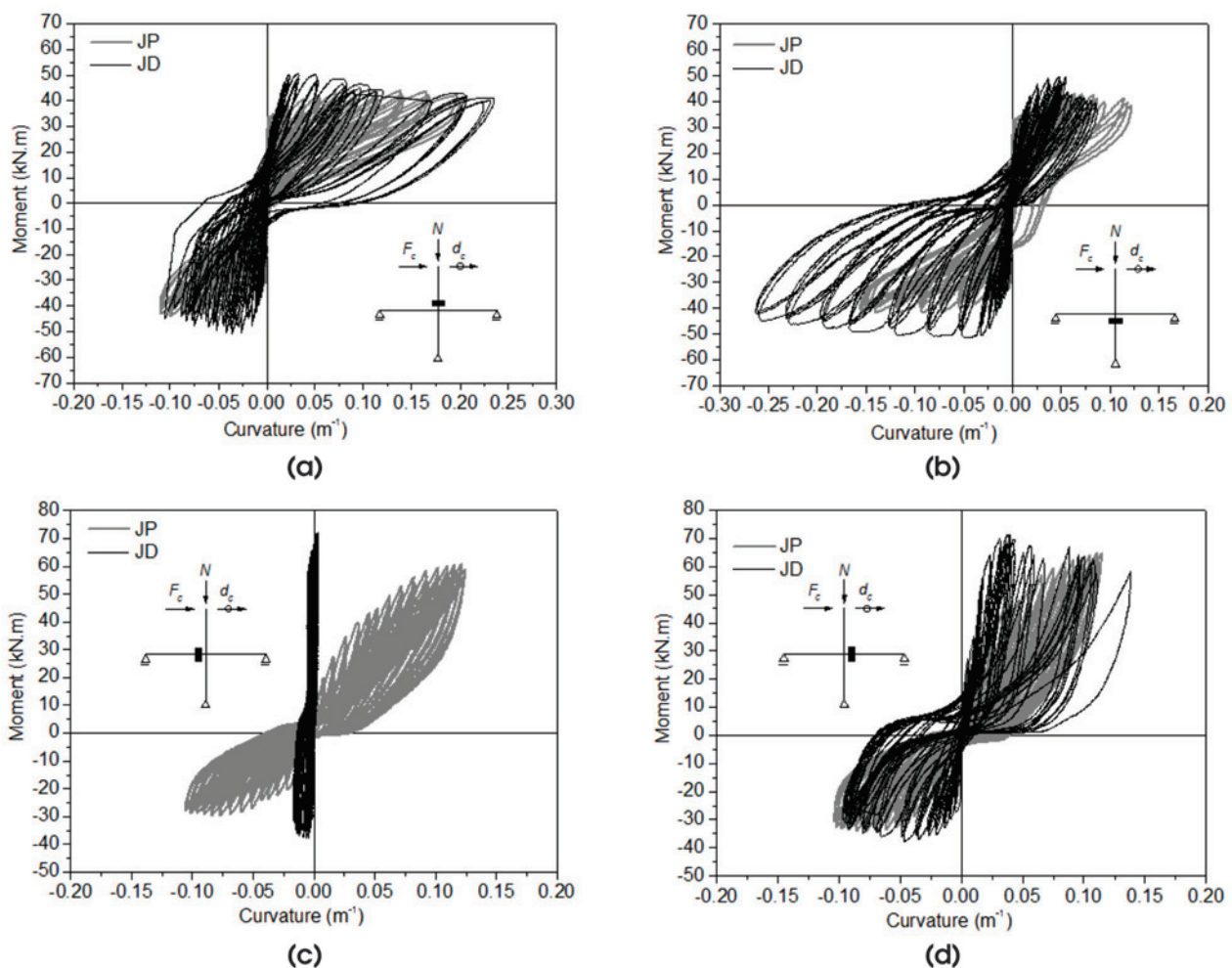
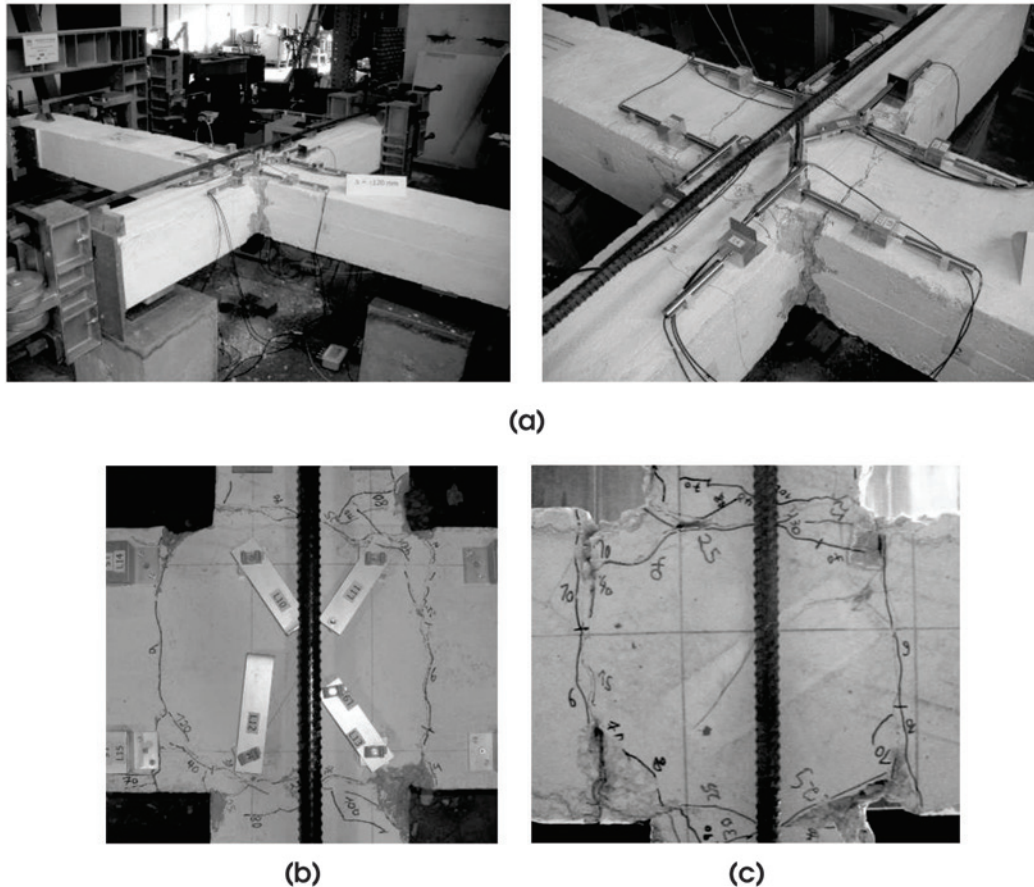


Figure 9 – Final damage state of specimen JP: a) general view; b) joint top face; c) joint bottom face



column-joint interfaces, without significant damage in the joint region. In this specimen were observed four main cracks, one at each beam-joint and column-joint interface.

In specimen JD a larger damage distribution was observed. Cracking began at the beam-joint and column-joint interfaces, spreading afterwards to the beam and column spans. Cracking and concrete cover spalling were observed in the joint region.

Figure 11 illustrates the crack pattern observed at the end of the test for the two specimens. As previously referred, the specimen with plain reinforcing bars displayed damage concentrated around the joint region, in opposition to the larger damage distribution observed for the specimen with deformed bars.

In Figure 12 and Figure 13 are represented the evolution of the relative displacements measured by the LVDTs placed near the joint region of specimens JP and JD, respectively. For specimen JP, the largest relative displacements in the beams and columns were registered at the interfaces with the joint region, by the LVDTs located at the first slice of each element (L14, L15, L16 and L17, in the beam; L10, L11, L12 and L13, in the column). For specimen JD, the largest relative displacements were also registered by these same LVDTs, except for L14 and L15. In general terms, larger relative displacements were registered for specimen JD. Namely, the

relative displacements measured at the columns of specimen JD are about two times the relative displacements measured at the columns of specimen JP. As expected and in accordance to what was observed, the diagonal LVDTs placed at the joint region of specimen JD registered significantly larger deformation in comparison to JP.

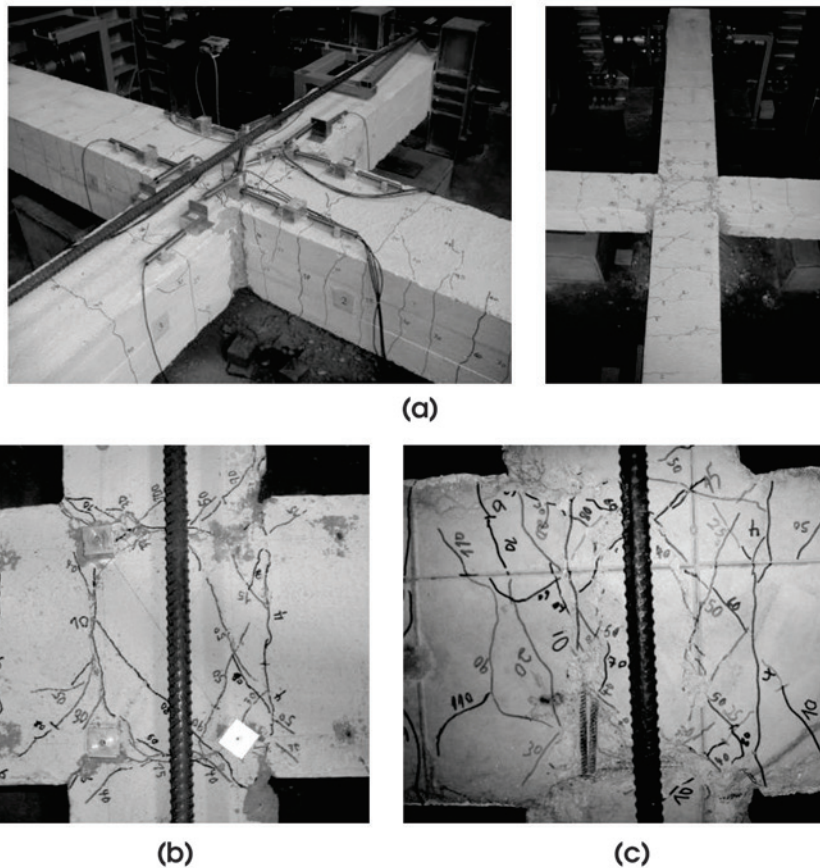
The lengths of the plastic hinges ( $L_p$ ) formed at the beam-joint and column-joint interfaces were estimated directly from the visual inspection of the damaged areas and are indicated in Table 3. The quotient ( $L_p/h$ ) between the plastic hinge length and the corresponding section depth ( $h$ ) are also presented. The estimated plastic hinges length is approximately  $0.25h$  and  $0.90h$  for specimens JP and JD, respectively. In other words, the plastic hinges length determined for specimen JD are about three times the plastic hinges length determined for specimen JP.

#### 4. Conclusions

The experimental work described in this paper is included in a larger experimental campaign being developed at the Civil Engineering Department of the University of Aveiro (Portugal). The main objective of this campaign is to evaluate the influence of the bond-slip



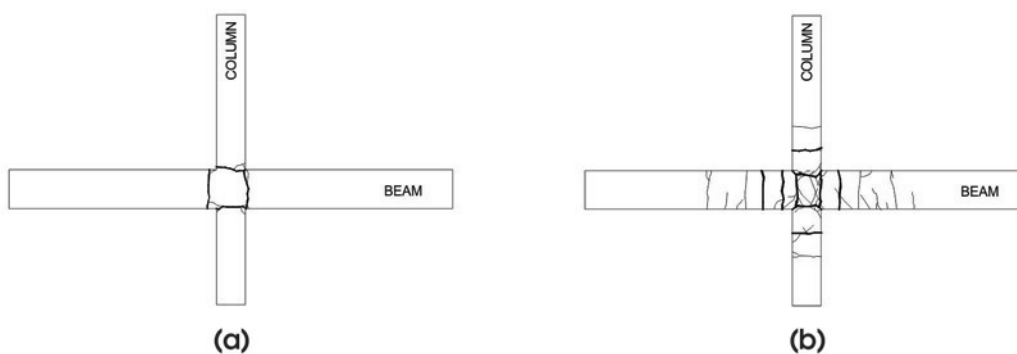
Figure 10 – Final damage state of specimen JD: a) general view; b) joint top face; c) joint bottom face



mechanism in the cyclic behavior of RC structural elements built with plain reinforcing bars, representative of existing RC buildings structures design and built without considering the seismic action. From the analysis of the experimental results presented in this paper, the following main conclusions can be drawn:

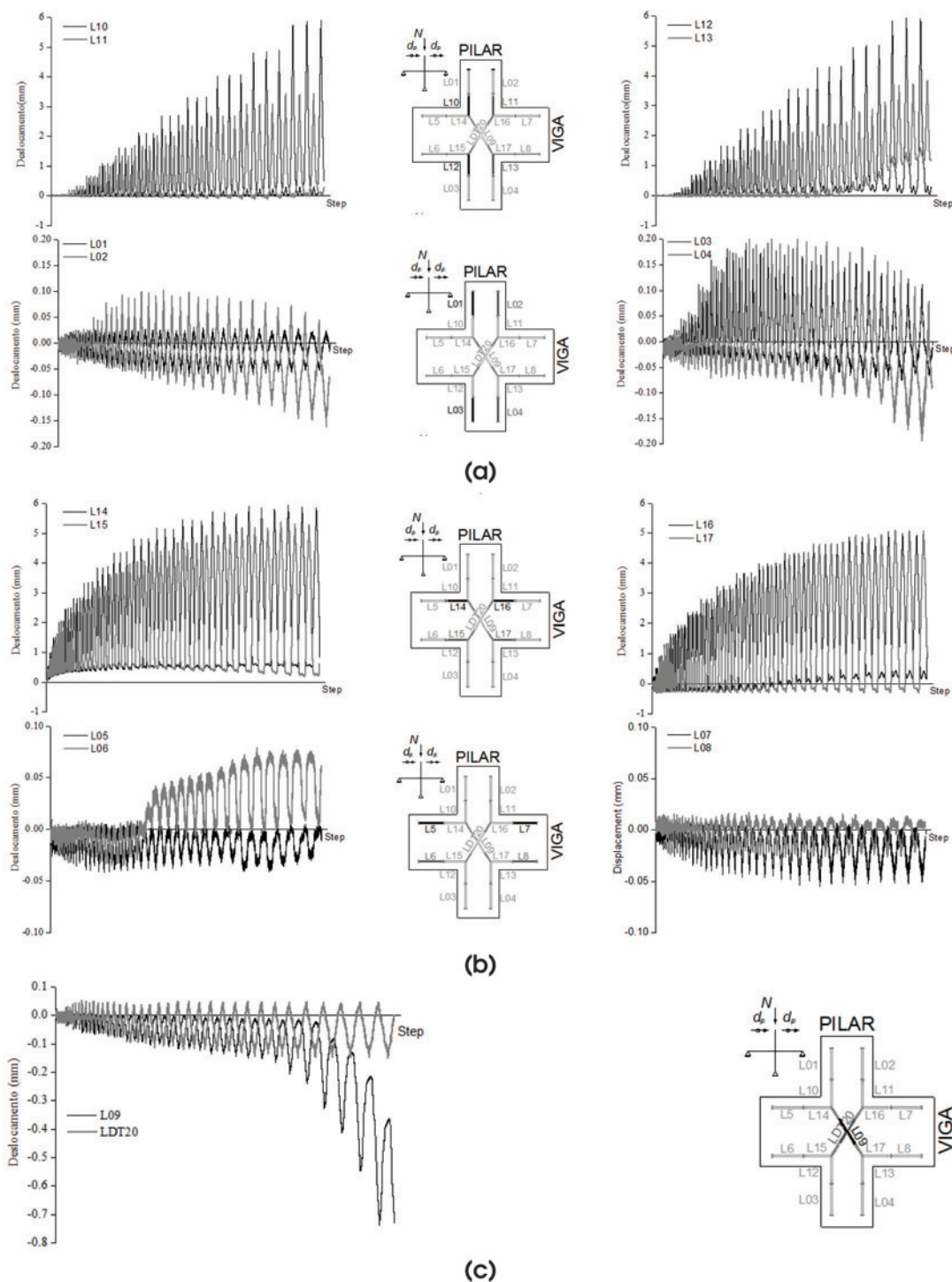
- The specimen with plain reinforcing bars (JP) displays lower maximum strength than the specimen with deformed bars (JD).
- Specimen JP displays smaller post-cracking stiffness than specimen JD.
- Until an imposed drift of 2%, the evolution of dissipated energy

Figure 11 – Final damage pattern (top face): a) specimen JP; b) specimen JD



- is similar for both specimens.
- The total energy dissipated by specimen JP is 10% lower than the total energy dissipated by specimen JD. This conclusion is in agreement to research work performed by other authors [1].
- Larger values of moment were determined for specimen JD. The effect of bond properties in the cyclic behavior of the beam-

Figure 12 - Relative displacement evolutions in specimen JP at: a) beam; b) column; c) joint



column joints was well illustrated by the differences registered between the damage evolution displayed by the two specimens. The specimen with plain reinforcing bars displayed damage concen-

trated around the joint region, mainly located at the beam-joint and column joint interfaces. Damage inside the joint region was negligible. Conversely, a larger damage distribution was observed for the

Figure 13 – Relative displacement evolutions in specimen JD at: a) beam; b) column; c) joint

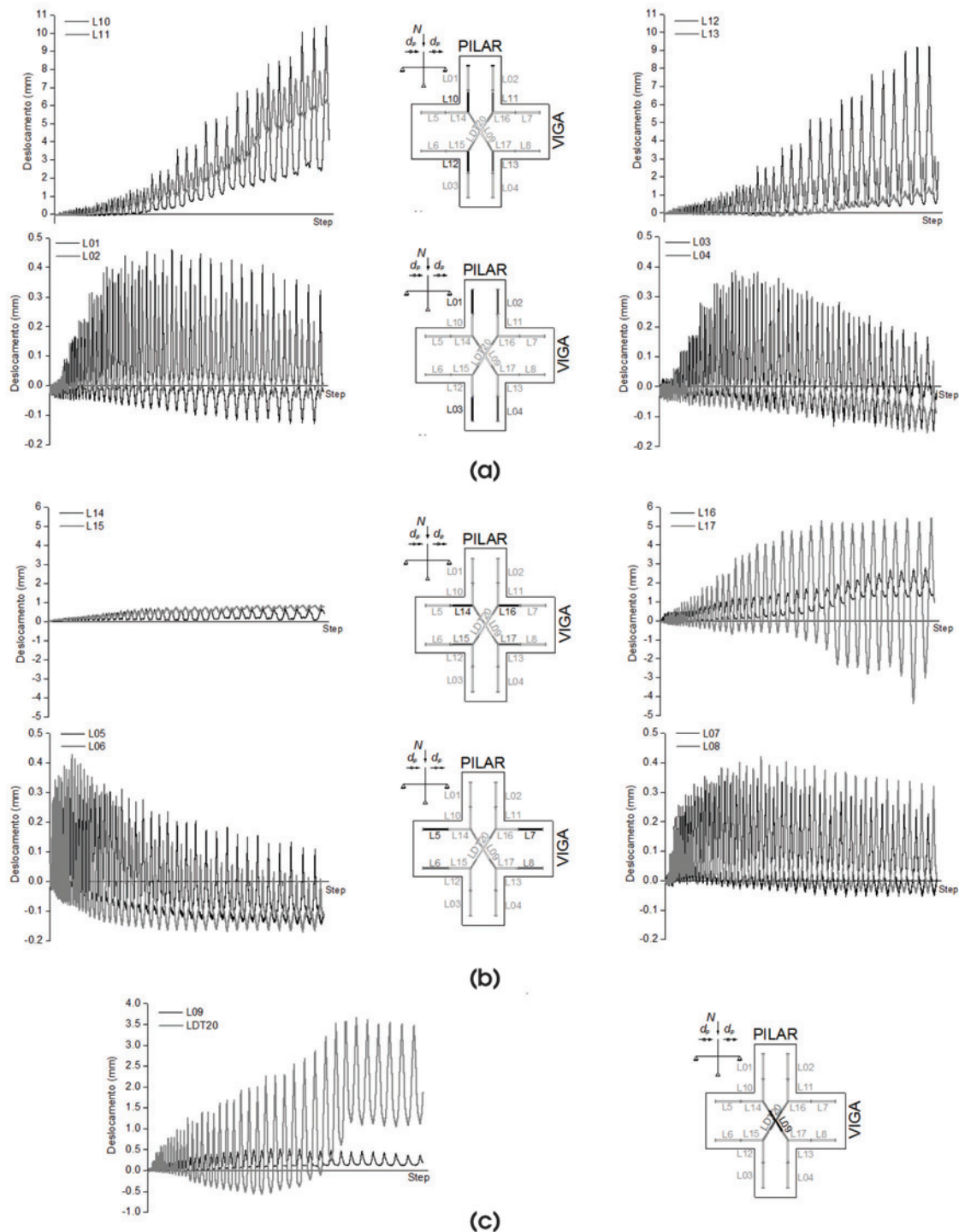


Table 3 - Plastic hinges length ( $L_p$ )

Element	Specimen JP		Specimen JD	
	$L_p$ (m)	$L_p/h$	$L_p$ (m)	$L_p/h$
Superior column	0.11	0.37	0.27	0.90
Inferior column	0.08	0.27	0.28	0.93
Left beam	0.10	0.25	0.36	0.90
Right beam	0.08	0.20	0.35	0.88

specimen with deformed bars, with spreading of cracks along the beam and column spans, and cracking and concrete cover spalling in the joint region. The different types of damage evolution resulted in significantly different plastic hinges length. The plastic hinges length estimated for the specimen with deformed bars are about three times the plastic hinges length determined for the specimen with plain bars.

## 5. Acknowledgments

This paper reports research developed under financial support provided by "FCT - Fundação para a Ciência e Tecnologia", Portugal, namely through the PhD grants of the first and second authors and Sabbatical Leave grant of the third author, with references SFRH/BD/27406/2006, SFRH/BD/62110/2009 and SFRH/BSAB/939/2009, respectively. Authors would like to acknowledge the following companies: (i) CIVILRIA, for the construction of the test specimens; and, (ii) SOMAGUE, GRUPO MENESES, SILVA TAVARES & BASTOS ALMEIDA and PAVIÚTIL, for the construction of the structural reaction systems. The authors also acknowledge Eng. António Figueiredo, Eng. Guilherme Carlos, Eng. Henrique Pereira and Eng. Hugo Rodrigues, for helping in the preparation of the test setup.

## 6. References

- [01] Varum, H. Seismic Assessment, Strengthening and Repair of Existing Buildings, Aveiro, Portugal, 2003, PhD Thesis - University of Aveiro, 508p.
- [02] Berra, M.; Castellani, A.; Ciccotelli, S. Bond-slip effects on reinforced concrete elements under earthquake loading. *European Earthquake Engineering*, v. 8, n. 3, 1994; p.3-10.
- [03] International Federation for Structural Concrete (CEB-FIB). Bulletin N.10 - Bond of reinforcement in concrete. State-of-art report prepared by Task Group Bond Models. Lausanne, Switzerland, 2000.
- [04] Fabbrocino, G.; Verderame, G. M.; Manfredi, G. C. Structural models of critical regions in old-type r.c. frames with smooth rebars. *Engineering Structures*, v. 26, 2004; p.2137-2148.
- [05] Fabbrocino, G.; Verderame, G. M.; Manfredi, G. Experimental behaviour of anchored smooth rebars in old type reinforced concrete buildings. *Engineering Structures*, v. 27, 2005; p.1575-1585.
- [06] Feldman, L. R.; Bartlett, F. M. Bond strength variability in pullout specimens with plain reinforcement. *ACI Structural Journal*, v. 102, n. 6, 2005; p. 860-867.
- [07] Verderame, G. M.; Ricci, P.; Carlo, G. D.; Manfredi, G. Cyclic bond behaviour of plain bars. Part I: Experimental investigation. *Construction and Building Materials*, v. 23, 2009; p. 3499-3511.
- [08] Liu, A.; Park, R. Seismic behaviour and retrofit of pre-1970's as-built exterior beam-column joints reinforced by plain round bars. *Bulletin of the New Zealand Society for Earthquake Engineering*, v. 34, n.1, 2001; p.68-81.
- [09] Pampanim, S.; Calvi, G. M.; Moratti, M. Seismic behaviour of RC beam-column joints designed for gravity loads. *In: Proceedings of the 12<sup>th</sup> European Conference on Earthquake Engineering*, London, 2002, Paper No. 726.
- [10] Verderame, G. M.; Fabbrocino, G.; Manfredi, G. Seismic response of r.c. columns with smooth reinforcement. Part II: Cyclic tests. *Engineering Structures*, v. 30, 2008; p.2289-2300.
- [11] Marefat, M. S.; Shirazi, S. M. H.; Rostamshirazi, R.; Khanmohammadi, M. Cyclic Response of Concrete Beams Reinforced by Plain Bars. *Journal of Earthquake Engineering*, v. 13, 2009; p.463-481.
- [12] Pinto, A. V.; Varum, H.; Molina, J. Experimental Assessment and Retrofit of Full-Scale Models of Existing RC Frames. *In: Proceedings of the 12<sup>th</sup> European Conference on Earthquake Engineering*, London, 2002, Paper No. 855.
- [13] Pinto, A. V.; Verzeletti, G.; Molina, J.; Varum, H.; Pinho, R.; Coelho, E. Pseudo-dynamic tests on non-seismic resisting RC frames (bare and selective retrofit frames). EUR Report No. 20244 EN, ELSA, JRC, EC, Ispra, Italy, 1999.
- [14] COMITÉ EURO-INTERNATIONAL DU BETÓN (CEB). RC elements under cyclic loading. State-of-the-art report, London: Thomas Telford, 1996, 190 p.
- [15] COMITÉ EURO-INTERNATIONAL DU BETÓN (CEB). Bulletin d'Information N. 217 - Selected justification notes, 1993.
- [16] Eligehausen, R.; Popov, E. P.; Bertero, V.V. Local bond stress-slip relationships of deformed bars under generalized excitation. Report No. UCB/EERC 82-23, Earthquake Engineering Research center, University of California, Berkeley, U.S.A., 1983.
- [17] Verderame, G. M.; Ricci, P.; Carlo, G. D.; Fabbrocino, G. Cyclic bond behaviour of plain bars. Part II: Analytical investigation. *Construction and Building Materials*, v. 23, 2009; p.3512-3522.
- [18] Prota, A.; Cicco, F.; Cosenza, E. Cyclic behavior of smooth steel reinforcing bars: experimental analysis and modeling issues. *Journal of Earthquake Engineering*, v. 13, 2009; p.500-519.

- [19] Fernandes, C.; Melo, J.; Varum, H.; Costa, A. Comportamento cíclico de nós viga-pilar com armadura lisa. *In*: Proceedings of the CINPAR 2010 - 6<sup>th</sup> International Conference on Structural Defects and Repair, Córdoba, Argentina, Paper Ref. 042.
- [20] INSTITUTO PORTUGUÊS DA QUALIDADE (IPQ). Portuguese Standard EN 206-1: Betão, Parte 1: Especificação, desempenho, produção e conformidade. Portugal, 2007.
- [21] EUROPEAN COMMITTEE FOR STANDARDIZATION (CEN). Eurocode 2: Design of Concrete Structures – Part 1-1: General rules and rules for buildings. Brussels, Belgium, 2004.